Electrically Enhanced Hydrogen Adsorption in Metal-Organic Frameworks

Liviu P. Zârbo,[*,†] Marius A. Oancea,[†,‡] Emmanuel Klontzas,[¶,§] Emmanuel Tylianakis,[‖,¶] Ioana G. Grosu,[†] and George E. Froudakis[¶]

†*Mol & Biomol Phys Dept, Natl Inst Res & Dev Isotop & Mol Technol, RO-400293 Cluj-Napoca, Romania.*

‡*Max Planck Institute for Gravitational Physics (Albert Einstein Institute), Am Mühlenberg 1, D-14476 Potsdam, Germany*

¶*Department of Chemistry, University of Crete, Voutes Campus, P.O. Box 2208, 71003 Heraklion, Crete, Greece*

§*Theoretical and Physical Chemistry Institute, National Hellenic Research Foundation, Vass. Constantinou 48, GR-11635 Athens*

‖*Materials Science and Technology Department, University of Crete, Vassilika Voutes, P.O. Box 2208, Heraklion, Greece*

E-mail: liviu.zarbo@itim-cj.ro
Phone: +40-264-584037/196

Abstract

Using a multiscale approach, we show that applied electric field does not affect significantly the hydrogen uptake of weakly polarizable metal-organic frameworks (MOFs). Nonetheless, we show that, for large MOF polarizabilities, the hydrogen uptake can double in applied electric field. We propose searching for a novel class of hydrogen storage materials, that of highly polarizable porous MOFs. Hydrogen uptake in such materials would be controlled by electric field, a much easier to adjust parameter than pressure or temperature.

1 Introduction

One of the top priorities of the modern economies is to secure the power sources and develop the extended energy distribution networks to satisfy the ever increasing energy demands. Nowadays and in the near future, fossil fuels are expected to play dominant role in providing the required energy for our needs mostly by converting to electricity or heat, since the relative technology has reached maturity and is used to power the vast majority of our daily activities. The restricted access to the resources of fossil fuels, coupled with the inevitable depletion of the underground reserves has spurred the quest for the development of alternative energy technologies. There are several alternative energy resources with economic potential, such as solar, wind, marine, geothermal and biomass. These provide energy for static applications, but they are inherently fluctuating, so they cannot fully replace traditional power plants. Efficient and cost effective high density energy storage solutions are intensely sought as the key for regularizing the output of alternative energy sources. But, such solutions would open the way for emission free mobile applications, sensibly reducing their environmental footprint. Among the possible high density energy storage solutions, using hydrogen as an energy carrier is regarded as one of the most promising. Hydrogen releases almost

three times more energy per unit of mass than gasoline,[1] and its combustion produces mainly water, which makes it ideal for environmentally friendly applications.

The exploitation of hydrogen in mobile applications includes three basic steps, namely the production of hydrogen, the storage of hydrogen and the conversion of hydrogen to power. The latter involves the fuel cell technology for splitting hydrogen molecule and producing power and water with high efficiency. There are three hydrogen storage technologies. The most mature ones, involving hydrogen storage as a compressed gas or as a liquid at cryogenic temperatures, seem to have reached their full potential. The third technology involves the storage of hydrogen in atomic or molecular form in the structure of materials. For reasons explained elsewhere,[1] hydrogen storage in materials has been intensely investigated as a potentially safer and more energy efficient alternative to the first two. Specific targets have been established concerning the reversible hydrogen capacity of materials containing storage tanks. To enable a driving range exceeding 300 miles for the hydrogen powered vehicles, DOE set targets[2] of 5.5% H_2 for the gravimetric, and 40g/L for the volumetric capacity of the whole on-board storage system. This means the deliverable uptakes of the material in the tank should exceed the capacities mentioned above.

Physical adsorption of molecular hydrogen in porous materials has been proposed as the most promising approach to reaching the DOE targets for hydrogen storage on-board of vehicles. Physisorption has the advantage of high reversibility and fast adsorption-desorption kinetics during the loading cycles. A variety of porous materials have been proposed[3] and studied both theoretically and experimentally, the most promising of them belonging to the family Metal-Organic Frameworks[4] (MOFs). These materials have been the subject of intense research over the last fifteen years because of their physico-chemical properties, such as high surface area, large pore volumes, and tunable chemical properties, identified as crucial for achieving high H_2 storage capacities. It has been proven that surface area and pore volume affect the H_2 storage capacities and their effect is more pronounced in different pressure ranges of the adsorption isotherms of the examined materials. A third important factor is the binding affinity of the molecular hydrogen to the pore surface. In contrast to the case of hydrides where hydrogen is absorbed in the atomic form with high absorption enthalpy (40-100kJ/mol), in physical adsorption H_2 interacts mainly through weak van der Waals interactions with the surface leading to weak adsorption enthalpies (4-12kJ/mol). Such low adsorption enthalpies prevent large capacities of adsorption at room temperature. Room temperature adsorption capacities are of the order of 1-2%wt, while at 77K and high pressures, the capacities are close to the established targets.[5] It has been estimated,[6,7] that for adsorption enthalpies in the range of 10 kJ/mol to 30kJ/mol, the DOE targets are attainable. The adsorption enthalpy can be enhanced by designing materials with certain pore sizes in the range of nanoporous materials and by controlling the chemical functionality of the pore surface and most of the efforts are focused on enhancing adsorption enthalpy. One must have in mind that the overall H_2 capacity would be a compromise of more than the three factors that have been mentioned above as has been shown recently by the construction of quantitative structure-property relationship (QSPR) models.[8]

Several routes have been proposed to enhance the adsorption strength of H_2 in physisorption materials. In the case of MOFs, these routes[9,10] include doping with species that can polarize H_2, such as lithium cations, the functionalization of linkers, the existence of open metal sites either on the inorganic building blocks or on the linker, the pore size control either by selecting linkers with various lengths or by catenation. Another route, that has not been considered yet in the case of MOFs, is the enhancement of the binding energy by applying an external electric field. Directly increasing the H_2 binding to sorbent materials via electric fields has been proposed only recently[11] and is still a largely unexplored area in hydrogen storage. The original proposal showed[11] that the hydrogen adsorption capacity of a BN sheet can be

tuned and enhanced by a sufficiently large applied electric field to meet the DOE requirements. Under the applied electric field, both H_2 and the adsorbent's surface get polarized, and the dipole-dipole interaction between the two induced dipoles enhances the binding. The idea originated from an earlier work[12] related to polarization-mediated binding of hydrogen to metal atoms. Subsequent theoretical investigations under applied electric field were performed on systems such as: i) carbon nanotubes decorated with metals,[13,14] SiC nanotubes,[15] ii) atomic clusters such as $C_{12}N_{12}$ isomers[16] or $(MgO)_9$ metal oxide clusters,[17] and iii) two-dimensional nanosheets such as graphene decorated with metals,[18–21] graphyne doped or decorated with metals,[22,23] B/C/N sheets,[24] AlN sheets[25] and metal decorated silicene.[26] To our knowledge, no one has approached this problem in MOFs, although there has been a proposal for building a three dimensional structure, a π-stacked organic crystal[27] with enhanced adsorption properties in electric field.

In this paper, we have chosen to investigate the adsorption of H_2 in IRMOF-1 in applied electric field. IRMOF-1 is one of the most investigated MOFs and its H_2 adsorption has been extensively studied both experimentally and theoretically. Theoretical investigations including quantum mechanics calculations and Grand Canonical Monte Carlo (GCMC) simulations have been performed to find the optimal configurations and the corresponding binding energies of hydrogen in the different adsorption sites of the material and to predict the adsorption capacity in different thermodynamic conditions. Literature reports[28,29] concerning quantum mechanics calculations can be divided in two groups based on the model that was used to represent IRMOF-1, either by performing calculations on fragments of various sizes taken from the crystal structure, or by taking into account the crystal with the corresponding periodic boundary conditions. It has been shown[28–30] that the strongest adsorption site is located on Zn_4O corner (known as the "cup" site, labeled[31] α) with an enthalpy of adsorption of -7.1kJ/mol, in good agreement with the available experimental value at 77K. The sites, labeled[31] β and δ, located on the Zn_4O corner and the site located on top of the phenyl ring, respectively, were found to be isoenergetic with a enthalpy of adsorption of -4.1 to -4.6kJ/mol. GCMC simulations on IRMOF-1 have been mainly performed at 77K and 298K and pressure ranges up to 150bar and were recently summarized by Durette *et al.*[32] The predicted uptakes showed small deviations from the value of 1.3%wt at 77K and 1 bar where larger deviations has been found for higher pressures (5.2 to 7.2%wt at 20bar). It was shown that quantum corrections are essential at 77K where the addition of partial charges was found to overestimate the uptake in some cases.

The rest of the paper is structured as follows. In Sec. 2, we provide the computational details used in our calculations. In Sec. 3 we present the results of our calculations. We justify the computational model used to obtain the H_2 uptake in electric field by quantum chemistry calculations on finite size IRMOF-1 models as presented in Sec. 3.1. Using results from periodic density functional (DFT) calculations, we parametrize a simple model used for GCMC calculations of H_2 adsorption isotherms in electric field, as presented in Sec. 3.2. We conclude in Sec. 4.

2 Computational Details

To investigate the adsorption in electric field on IRMOF-1, we employed a multiscale methodology[33] that was modified to include electrically induced polarization effects. Our approach was as follows. i) We performed *ab initio* calculations of the binding energy vs the distance of H_2 to the binding sites of IRMOF-1, with and without electric field. In these calculations, the binding sites were represented by finite size fragments containing these sites. ii) We performed periodic structure DFT simulations of the IRMOF-1 unit cell with and without electric field to obtain: optimized lattice parameters, Born effective charges for each atom and the atomic positions in unit cell. iii) Using the data from the ab initio calculations, GCMC simulations were performed to obtain the H_2

uptake at 77K and 300K.

The calculations i) are described in Sec.3.1. Each binding site was modeled by a finite fragment of IRMOF-1. We formed dimers in which one monomer is the MOF fragment, and the other is a H_2 molecule. The binding energies of H_2 to a binding site were computed with respect to the distance between that site and the center of the H_2 molecule. Each monomer is relaxed with and without electric field, and then the dimer binding energies are computed. The calculations were done at the B3-LYP[34] level of theory with the def2-TZVP[35] basis set. Dispersion corrections[36] with Becke-Johnson damping[37] were taken into account. We also corrected for the basis set superposition errors using the counterpoise method.[38] The energy and geometrical tolerance criteria, for the structure optimizations of monomers and dimers, carried out in this work and its attached Supplementary Information (SI), have been set to 10^{-8}a.u. and 10^{-4}a.u., respectively. The cluster calculations have been performed using the TURBOMOLE software package.[39]

The GCMC calculations of the adsorption isotherms used data from ii) periodic structure DFT calculations, performed using the software CRYSTAL09.[40] The calculations were done at GGA-PBE[41] level using all electron Gaussian basis sets. We considered the basis pob-TZVP,[42] which is based on def2-TZVP. This choice of functional/basis set is justified because: a) the Born effective charges (or atomic polarizations) computed for Zn and O in the structure agree to those of ZnO, b) the static dielectric constant (permittivity) $\kappa = 1.41$ is in very good agreement with the value $\kappa = 1.37$ estimated using the Clausius-Mossotti approach,[43] and c) the calculated electronic band gap $E_g = 3.6\,\mathrm{eV}$ only slightly overestimates the experimental[44] value $E_g = 3.4\,\mathrm{eV}$. As previously shown,[45,46] the dynamical Born effective charges are not very sensitive to the different exchange-correlation functionals used to estimate them.

The optimized lattice constants and Born charges were computed using a $6 \times 6 \times 6$ k-point grid in the Brillouin zone of the IRMOF-1 fcc cell with 106 atoms/cell. For consistency, in the GCMC simulations, we used the lattice parameters obtained from our calculations. Those are $a = b = c = 26.06$Å for zero field and $c = 26.07$Å in applied field. These values are slightly larger than the experimental ones as GGA-PBE typically overestimates the lattice parameters. The atomic relaxations, in the presence of the field, are performed using a $2 \times 2 \times 1$ mesh of k-points in the Brillouin zone of $1 \times 1 \times 2$ cubic supercell following an approach[45] proposed for periodic system relaxation in electric field.

The self-consistent-field periodic structure calculations were considered to be converged when the energy changes between interactions were smaller than 10^{-8}a.u. An extra-large predefined pruned grid consisting of 75 radial points and 974 angular points was used for the numerical integration of charge density. Full optimizations of the lattice constants and atomic positions have been performed with the optimization convergence of 5×10^5Hartree/Bohr in the root-mean square values of forces and 1.2×10^3Bohr in the root-mean square values of atomic displacements. The level of accuracy in evaluating the Coulomb and exchange series is controlled by five parameters.[40] The values used in our calculations are 7, 7, 7, 7, and 14.

The adsorption isotherms were computed performing iii) GCMC simulations using the RASPA2 program.[47] The program was modified to allow for the inclusion of the H_2 dipole interaction with the applied electric field. The framework is considered immobile for both cases, with and without applied electric field. The cut-off radius is set to 12.8Å, the lattice constants and positions are those obtained from the periodic structure calculations. For non-bonded interactions we use the Lennard-Jones potential with the parameters taken from the DREIDING[48] force field for all the framework atoms. The partial charges for the framework atoms and H_2, as well as the Lennard-Jones coefficients are listed in SI. The atomic positions and Born charges, also listed in SI, were obtained from the ii) periodic structure calculations discussed above.

3 Results and discussion

The magnitude of the H_2 uptake increase in MOF will depend on the magnitude of the applied field. In our calculations, we included the effects of polarization on both the adsorbate and the adsorbent. H_2 is weakly polarizable and possesses no permanent dipole moment.[49] IRMOF-1 is also weakly polarizable, with an estimated permittivity[43] $\kappa = 1.37$. Thus, one needs a large electric field to significantly increase the uptake. However, too large applied fields $E = 0.045\,\text{a.u.} = 23\,\text{GV/m}$, as those considered in the original study[11] on BN sheets, would cause the Zener breakdown of the MOF. An upper limit for the Zener breakdown field of IRMOF-1 can be estimated[50] at $\sim E_g/a = 13\,\text{GV/m}$, where $E_g = 3.4\,\text{eV}$ is the experimental value of the band gap,[44] and a is the lattice constant of the cubic IRMOF-1 cell. Therefore, we choose $E_0 = 0.005\,\text{a.u.} = 2.57\,\text{GV/m}$ as the magnitude of the applied electric field throughout our simulations.

In our model, we consider a spherical IRMOF-1 crystallite on which we apply the electric field $E_0\hat{z}$. The adsorbed gas feels the effect of the field through the local field inside of the pore. The contributions to the local field inside the pore are[51] the applied field E_0, the depolarization and the Lorentz fields, plus the field of the atomic charges. For a spherical MOF crystallite, the Lorentz and the depolarization field cancel each other. Thus, we can approximate the field in the center of the pore by E_0. To simplify our treatment, in all our subsequent calculations, we assumed that the electric field induced inside the MOF pores was constant, equal to the applied field E_0. As a result, the molecule of H_2 inside the pore would be subjected to a field equal to E_0 plus the contributions of the charge distribution inside the MOF.

3.1 Quantum chemistry calculations

We perform DFT simulations to obtain the interaction energy between the H_2 molecules and their binding sites as a function of distance in applied electric field $E_0 = 0.005$a.u.. We consider the three adsorption sites[31] referenced at the end of Sec. 1 for the hydrogen in MOF: the δ-site above the center of the benzene dicarboxylate (BDC) linker, and the α "cup" and β adsorption sites, located on the secondary building unit (SBU), as shown in Fig. 1. Our scans are performed for $\pm E_0\hat{z}$ field and the results are compared to the ones in the zero field case. The hydrogen molecule is parallel to the z-axis in the case presented in Fig. 1. The MOF fragments (clusters) used in this calculation are shown next to each plot in Fig. 1a the linker and two hydrogen terminated SBU units, in Fig. 1b the SBU unit modeling the "cup" site, and in Fig. 1c) the SBU unit modeling the β site.

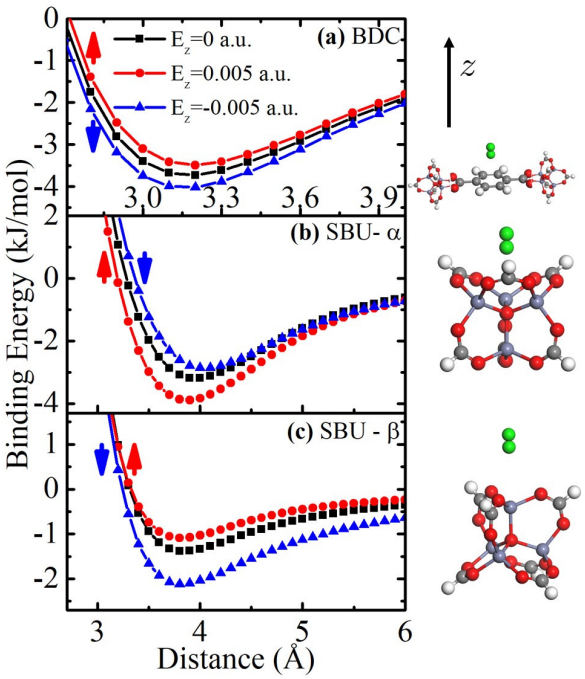

Figure 1: Potential energy curves for H_2 adsorbed at a) the δ-site at the center of the BDC linker, b) the α "cup" site, c) the β site. The positive direction is considered $\hat{z}$-direction. The electric field is color coded red for positive and blue for negative. The horizontal axis of the graph represents the distance between the center of the H_2 molecule and a) center of the benzene ring on the linker, b) the μ_3-O atom in the center of the SBU, c) the Zn atom above the μ_3-O from the center of the SBU. The Zn, C, O and H atoms of the fragments are colored purple, gray, red and white, respectively. The adsorbed H_2 is colored green.

The potential energy curves in Fig. 1 show that the binding energy is either enhanced, or decreased depending on the field direction. This effect has been noticed in previous work on Li-decorated carbon nanotubes[13] and graphene.[18] Induced dipole-dipole interaction does not explain this feature, as both H_2 and MOF dipoles are odd functions of the electric field, so the dipole-dipole interaction is even. It has been argued[52] that the binding of H_2 to the sites in IRMOF-1, in zero field, is mostly due to dispersion forces. This suggests that the energy differences seen in Fig. 1 can be explained by considering polarization effects. We do so below, but only for the electrostatic energies and not for exchange and correlation.

To show this, we calculate the lowest order terms in the multipole expansion of the electrostatic energy for the system formed by the BDC linker and H_2. The benzene ring (monomer A) is representative for the BDC fragment and its center is the origin. The H_2 molecule (monomer B) is above the center of the ring as in Fig. 1a at position $\mathbf{R} = R\hat{z}$. The field is $\pm E_0\hat{z}$.

We compute the components of the dipole $p_\alpha^{A,B}$ and quadrupole $\Theta_{\alpha\beta}^{A,B}$ moments in the applied field for each isolated monomer from wavefunctions. The applied field E_0 induces a dipole in each monomer, but is too small to affect significantly the quadrupole moments (see the SI for more details). Thus, the additional electrostatic energy terms due to the polarization induced by electric field are a dipole-dipole term (DD) and two quadrupole-dipole terms (DQ and QD). This follows from the multipole expansion[53] of the electrostatic energy for two monomers A, and B

$$\begin{aligned} U_{AB} &= \mathrm{DD} + \mathrm{DQ} + \mathrm{QD} \\ &= -T_{\alpha\beta}^{AB} p_\alpha^A p_\beta^B \\ &\quad -\tfrac{1}{3} T_{\alpha\beta\gamma}^{AB} (p_\alpha^A \Theta_{\beta\gamma}^B - \Theta_{\alpha\beta}^A p_\gamma^B) + \ldots , \end{aligned} \tag{1}$$

where $T_{\alpha\beta\ldots\nu}^{AB} = \nabla_\alpha \nabla_\beta \ldots \nabla_\nu 1/R$ in a.u. The Greek letters label the x-, y-, or z-axes.

Using Eq. (1), we compute the electrostatic energy terms DD, DQ, and QD. The results are shown in Fig. 2a. The dipole-dipole term is always attractive, but the DQ and QD terms are repulsive if the field is positive and attractive for

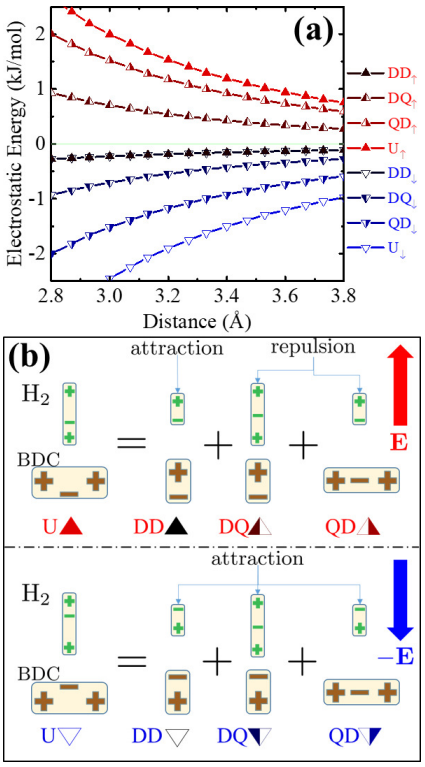

Figure 2: Electrically induced electrostatic interaction energy between benzene and H_2 vs. distance: a) calculated dipole-dipole (DD) and dipole-quadrupole (DQ, QD) terms of Eq. (1), b) pictorial explanation of the result. The DD terms are always attractive (negative), but too small compared to the QD and DQ terms which switch the sign if the electric field direction is reversed. As a result, the total electrostatic energy is repulsive for field $E_0\hat{z}$ and attractive and slightly larger for field $-E_0\hat{z}$. This is consistent with what is seen in Fig. 1a. The benzene is oriented as BDC in Fig. 1a, and its center is the origin, while H_2 position is $R\hat{z}$.

negative electric field. This is consistent with the result in Fig. 1a. For the small fields considered, the DD interaction is one order of magnitude smaller than QD and DQ interactions simply because the induced dipole is too small. This is true despite the fact that DD $\sim 1/R^3$ while DQ, QD $\sim 1/R^4$. The results of Fig. 1b, c, can be similarly explained, but one has to use atomic site-resolved charges and multipoles, rather than the global multipoles, for the short range interactions.

We performed additional tests by repeating the calculations presented in Fig. 1 with a meta-

GGA functional, namely M06-2x,[54] recently tested on IRMOF-1.[29] As discussed in SI, and similar to the result in Fig. 1, the binding energies in the electric field increase or decrease depending on the orientation of the field. But, in the case of some binding sites, the sign of the binding energy change with respect to the zero field case is opposite to the result obtained employing B3-LYP. This result is also opposite to what we expect from our electrostatics considerations. This could stem from the larger percentage of Hartree-Fock exchange M06-2x compared to B3-LYP, or could be an artifact of the meta-GGA functionals being constructed with the aid of electron density gradients. However, further benchmarking studies are needed to clarify what are the ideal functionals to use when studying metal-organic systems in electric field.

3.2 GCMC calculations in electric field

Paragraph 20 Based upon the insight offered by the *ab initio* calculations, we make a model for the adsorbent-adsorbate system formed by IRMOF-1 and H_2 gas in electric field. As discussed above, inside the pores of IRMOF-1 the field can be approximated as being equal to the applied field $E_0\hat{z}$. In our GCMC simulations, the adsorbent is represented by a periodic fcc IRMOF-1 unit cell of 424 atoms (see SI for details). Though relatively small, the applied electric field considered slightly deforms and polarizes the unit cell. Since the deformation of the unit cell is small compared to the cell size, we expect it not to affect significantly the H_2 uptake. The induced dipole moment of the unit cell is expected to influence the adsorption, so each atom in the model of IRMOF-1 for the GCMC calculation will carry both a partial charge and a dipole, as explained below. The hydrogen, on the other hand, will be weakly polarized by the field inside the pores. We model it as gas whose molecules can be polarized either parallel, or perpendicular to their axes. Without the applied electric field, our model reduces to the one previously used in GCMC simulations of H_2 adsorption on IRMOF-1.[55]

To make a polarized model for the adsorbate, we start from the unpolarized model, and introduce the polarization. The unpolarized H_2 molecule is modeled as[56] a quadrupole with charge $q \approx 0.468e$ on the H sites and $-2q$ at its center. In electric field, this molecule becomes polarized, depending on its orientation with respect to the field in the pore.[49] To account for this effect, we consider the adsorbate as made of two components: ${H_2}^{\parallel}$ with a constant polarization along its axis and ${H_2}^{\perp}$ with a constant polarization perpendicular to its axis. In the field E_0 present in the pores, the adsorbate molecule oriented along the field ${H_2}^{\parallel}$ has a dipole $p_{\parallel} = 0.033$a.u., and the molecule perpendicular to the field ${H_2}^{\perp}$ possesses a moment $p_{\perp} = 0.013$a.u.. To account for these dipoles, we place additional charges $\pm\delta q$ on the H sites of ${H_2}^{\parallel}$, chosen to reproduce $p_{\parallel}$. For ${H_2}^{\perp}$, only the center of H_2 is displaced perpendicular to the axis of the molecule by δd chosen to reproduce $p_{\perp}$. The numerical values of charges and distances for this model are given in the SI.

As in the case of the adsorbate, the polarized model for IRMOF-1 starts from the unpolarized model typically used in GCMC simulations. In the unpolarized model, each atom i is placed at the position $\mathbf{R}_i$ in the 424 atom unit cell. These positions are obtained, as explained in Sec.2, by optimizing the crystalline structure. To each atom i we assign a partial charge q_i and two Lennard-Jones coefficients $C^i_{6,12}$.

In the polarized model, each atom is displaced by the electric field to a new position $\mathbf{R}_i(E_0)$. These positions are also obtained by performing periodic structure optimization calculations in electric field. From the calculated value of the Born charge Z^*_i for each atom i, we can find the dipole moment acquired under the effect of the electric field as $\mathbf{p}_i = Z^*_i(\mathbf{R}_i(E_0) - \mathbf{R}_i)$. The simplest way to introduce these moments into the calculation, is by placing dummy charge sites next to each atom i, the charge of each site being labeled Q_i. Thus, we assign the charge $q_i - Q_i$ and position $\mathbf{R}_i$ to the atomic site i, and place the dummy charge $\mathbf{R}_i$ at $\mathbf{R}_i + \mathbf{d}_i$. The distance $\mathbf{d}_i$ and the charge $Q_i > 0$ are chosen so that $\mathbf{p}_i = Q_i\mathbf{d}_i$. We take $|\mathbf{d}_i| = 0.27$Å, which is an order of magnitude less than the equilibrium

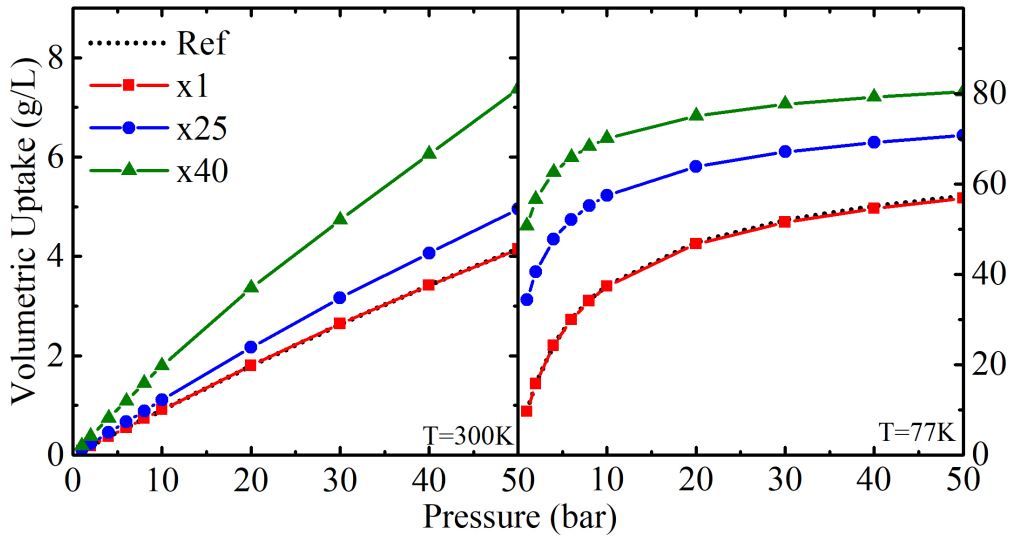

Figure 3: Absolute uptake for IRMOF-1 in applied electric field (red). The dotted line is the isotherm in the absence of electric field. The blue and green lines represent the cases with 25 and 40-fold increase of polarizability, respectively.

distances between H_2 and its adsorption sites, so we do not expect large spurious effects from the quadrupole-H_2 dipole terms. The dispersion coefficients are approximated to be identical to the ones in the zero field case.

We compute first the isotherms in zero field. Then, we use the polarized models for the adsorbate and IRMOF-1 to compute the isotherms at 300K and 77K in electric field. The positions $\mathbf{R}_i$ of atoms i are identical, in reduced coordinates, for both zero and non-zero field. The cut-off radius is set to 12.8Å. During the simulations, translation, rotation, insertion and deletion moves are performed on the H_2 molecules. The moves are modified to include the additional $-\mathbf{E}\cdot\mathbf{P}_{H_2}$ term which arises when the electric field is applied. As explained above, the local field in the pore is approximately $\mathbf{E}_0\hat{z}$.

The adsorption isotherms, shown in Fig. 3, are very close to the reference values without electric field. This is expected as only the induced dipole-dipole interaction increases the binding energy. As suggested by the results presented in Fig. 1, larger quadrupole-dipole terms are present, but according to our pictorial explanation of Fig. 2b, they cancel out. For each binding site in IRMOF-1, one could generate an identical binding site by a reflection operation. Assume a H_2 binds at the top of the first site, and another H_2 binds at the bottom of the second, where bottom-top is the z-direction. As in Fig. 2a, the dipole quadrupole contributions to the energy (DQ, QD) for the first site would have the opposite sign to the ones for the second (see SI for a more detailed explanation). Thus, the overall contribution to the uptake is only given by the dipole-dipole interaction, despite the optimistic expectations suggested by the results of Fig. 1. This contribution is small, as it is proportional to the square of the applied field.

As the electric field cannot be increased in a practical device too far beyond the already large value E_0 considered, one should search for more polarizable porous MOFs whose uptake can be electrically enhanced. To test this idea, we scale up the Born charges of IRMOF-1 25 and 40 times and repeat the GCMC simulations. As shown in Fig. 3, the hydrogen uptake at room temperature almost doubles for the 40-fold increase in polarizability. Such polarizable MOFs do exist,[57] but they are usually not porous. For porous isoreticular MOFs, lower permittivities, up to $\kappa = 1.94$, were estimated.[43] More research is needed to find a MOF that is both polarizable and highly porous.

4 Conclusions

We have chosen IRMOF-1 to test the potential of applied electric field to enhance H_2 uptake in MOFs. We provided an extension to the multiscale approach[33] previously used by some of us for adsorption simulations, which enables the inclusion of polarization effects in the GCMC simulations. We found that, apart from the expected induced dipole-dipole contribution to the interaction, higher order terms, such as dipole-quadrupole, contribute to the extra-binding in electric field. However, these terms change sign with the field direction, so they cancel out in the adsorption simulations. We have chosen the applied field as large as possible without causing the dielectric breakdown of the MOF. It appears that even this field is too low to significantly affect the hydrogen uptake. However, we showed that a 40-fold increase in IRMOF-1 polarizability would lead to an almost doubling of the uptake at room temperature. Thus, we believe that the only way to make further progress, in enhancing the hydrogen uptake in MOFs via electric fields, is to search for materials with both large pores and polarizability. Through this work, we propose opening a new research direction, that of electrically controlled adsorption in highly polarizable porous MOFs.

Acknowledgement L. P. Z. has been funded by a grant of the Romanian National Authority for Scientific Research and Innovation, CNCS-UEFISCDI, project number PN-II-RU-TE-2014-4-1309. E. K. has been funded by State Scholarships Foundation (SSF), grant number 2016-050-0503-8189, and co-financed by the European Union (European Social Fund-ESF) and Greek national funds through the action entitled "Reinforcement of Postdoctoral Researchers", in the framework of the Operational Programme "Human Resources Development Program, Education and Lifelong Learning" of the National Strategic Reference Framework (NSRF) 2014-2020. I. G. G. has been financially supported by the Romanian National Authority for Scientific Research and Innovation (ANCSI) through the Core Program, Project PN19-35-02-02. L. P. Z. thanks Gabriela Blăniţă, Dan Lupu, Atilla Bende, Claudiu Filip and Alston J. Misquitta for stimulating discussions, and David Dubbeldam for correspondence.

References

(1) Schlapbach, L.; Zuttel, A. Hydrogen-storage materials for mobile applications. *NATURE* **2001**, *414*, 353–358.

(2) USDOE, O. o. E. E.; Energy, R.; FreedomCAR, T.; Partnership, F. DOE targets for onboard hydrogen storage. *http://energy.gov/eere/fuelcells/downloads/doe-targets-onboard-hydrogen-storage-systems-light-duty-vehicles* **2013**,

(3) Jena, P. Materials for Hydrogen Storage: Past, Present, and Future. *The Journal of Physical Chemistry Letters* **2011**, *2*, 206–211.

(4) Suh, M. P.; Park, H. J.; Prasad, T. K.; Lim, D.-W. Hydrogen Storage in Metal-Organic Frameworks. *Chemical Reviews* **2012**, *112*, 782–835, PMID: 22191516.

(5) Murray, L. J.; Dinca, M.; Long, J. R. Hydrogen storage in metal-organic frameworks. *Chem. Soc. Rev.* **2009**, *38*, 1294–1314.

(6) Bhatia, S. K.; Myers, A. L. Optimum Conditions for Adsorptive Storage. *Langmuir* **2006**, *22*, 1688–1700, PMID: 16460092.

(7) Bae, Y.-S.; Snurr, R. Q. Optimal isosteric heat of adsorption for hydrogen storage and delivery using metal-organic frameworks. *Microporous and Mesoporous Materials* **2010**, *132*, 300 – 303.

(8) Bobbitt, N. S.; Chen, J.; Snurr, R. Q. High-Throughput Screening of Metal-Organic Frameworks for Hydrogen Storage at Cryogenic Temperature. *The Journal of Physical Chemistry C* **2016**, *120*, 27328–27341.

(9) Han, S. S.; Mendoza-Cortes, J. L.; Goddard III, W. A. Recent advances on simulation and theory of hydrogen storage in metal-organic frameworks and covalent organic frameworks. *Chem. Soc. Rev.* **2009**, *38*, 1460–1476.

(10) Klontzas, E.; Tylianakis, E.; Froudakis, G. E. On the Enhancement of Molecular Hydrogen Interactions in Nanoporous Solids for Improved Hydrogen Storage. *The Journal of Physical Chemistry Letters* **2011**, *2*, 1824–1830.

(11) Zhou, J.; Wang, Q.; Sun, Q.; Jena, P.; Chen, X. S. Electric field enhanced hydrogen storage on polarizable materials substrates. *Proceedings of the National Academy of Sciences* **2010**, *107*, 2801–2806.

(12) Niu, J.; Rao, B. K.; Jena, P. Binding of hydrogen molecules by a transition-metal ion. *Phys. Rev. Lett.* **1992**, *68*, 2277–2280.

(13) Liu, W.; Zhao, Y. H.; Li, Y.; Lavernia, E. J.; Jiang, Q. A reversible switch for hydrogen adsorption and desorption: electric fields. *Phys. Chem. Chem. Phys.* **2009**, *11*, 9233–9240.

(14) Zhang, Z.-w.; Li, J.-c.; Jiang, Q. Density functional theory calculations of the metal-doped carbon nanostructures as hydrogen storage systems under electric fields: A review. *Frontiers of Physics* **2011**, *6*, 162–176.

(15) Masumian, E.; Hashemianzadeh, S. M.; Nowroozi, A. Hydrogen adsorption on SiC nanotube under transverse electric field. *Physics Letters A* **2014**, *378*, 2549 – 2552.

(16) Mondal, S.; Srinivasu, K.; Ghosh, S. K.; Chattaraj, P. K. Isomers of C12N12 as potential hydrogen storage materials and the effect of the electric field therein. *RSC Adv.* **2013**, *3*, 6991–7000.

(17) Yin, Y.-H.; Chen, H.-S. The electric field effect on the hydrogen storage properties of (MgO)9. *Computational and Theoretical Chemistry* **2016**, *1081*, 1 – 8.

(18) Liu, W.; Zhao, Y.; Nguyen, J.; Li, Y.; Jiang, Q.; Lavernia, E. Electric field induced reversible switch in hydrogen storage based on single-layer and bilayer graphenes. *Carbon* **2009**, *47*, 3452 – 3460.

(19) Lee, S.; Lee, M.; Chung, Y.-C. Enhanced hydrogen storage properties under external electric fields of N-doped graphene with Li decoration. *Phys. Chem. Chem. Phys.* **2013**, *15*, 3243–3248.

(20) Zhang, X.; Tang, C.; Jiang, Q. Electric field induced enhancement of hydrogen storage capacity for Li atom decorated graphene with Stone-Wales defects. *International Journal of Hydrogen Energy* **2016**, *41*, 10776 – 10785.

(21) Tang, C.; Zhang, X.; Zhou, X. Most effective way to improve the hydrogen storage abilities of Na-decorated BN sheets: applying external biaxial strain and an electric field. *Phys. Chem. Chem. Phys.* **2017**, *19*, 5570–5578.

(22) Zhang, L.; Wang, N.; Zhang, S.; Huang, S. The effect of electric field on hydrogen storage for B/N-codoped graphyne. *RSC ADVANCES* **2014**, *4*, 54879–54884.

(23) Zhang, L.; Zhang, S.; Wang, P.; Liu, C.; Huang, S.; Tian, H. The effect of electric field on Ti-decorated graphyne for hydrogen storage. *Computational and Theoretical Chemistry* **2014**, *1035*, 68 – 75.

(24) Guo, J.-H.; Zhang, H. The effect of electric field on hydrogen storage for B/C/N sheets. *Structural Chemistry* **2011**, *22*, 1039.

(25) Yang, W.; Huang, R.; Liu, L.; Wang, L.; Zhang, R.; Zheng, Y.; Wang, Y. Double layers of H2 adsorption on an AlN sheet induced by electric field. *Journal of Nanoparticle Research* **2012**, *14*.

(26) Song, E. H.; Yoo, S. H.; Kim, J. J.; Lai, S. W.; Jiang, Q.; Cho, S. O. External electric field induced hydrogen storage/release on calcium-decorated single-layer and bilayer silicene. *Phys. Chem. Chem. Phys.* **2014**, *16*, 23985–23992.

(27) Liu, Z. Pi–Stacked organic molecular crystals under electric fields as viable storage media for molecular hydrogen. *International Journal of Hydrogen Energy* **2012**, *37*, 11842–11845.

(28) Sillar, K.; Hofmann, A.; Sauer, J. Ab Initio Study of Hydrogen Adsorption in MOF-5. *Journal of the American Chemical Society* **2009**, *131*, 4143–4150, PMID: 19253977.

(29) Wu, J.; Kucukkal, M. U.; Clark, A. E. H2 Adsorbed Site-to-Site Electronic Delocalization within IRMOF-1: Understanding Non-Negligible Interactions at High Pressure. *Materials* **2016**, *9*, 578.

(30) Klontzas, E.; Mavrandonakis, A.; Froudakis,; Carissan, Y.; Klopper, W. Molecular Hydrogen Interaction with IRMOF-1: A Multiscale Theoretical Study. *The Journal of Physical Chemistry C* **2007**, *111*, 13635–13640.

(31) Rowsell, J. L. C.; Yaghi, O. M. Strategies for Hydrogen Storage in Metal-Organic Frameworks. *Angewandte Chemie International Edition* **2005**, *44*, 4670–4679.

(32) Durette, D.; Bénard, P.; Zacharia, R.; Chahine, R. Investigation of the hydrogen adsorbed density inside the pores of MOF-5 from path integral grand canonical Monte Carlo at supercritical and subcritical temperature. *Science Bulletin* **2016**, *61*, 594–600.

(33) Tylianakis, E.; Klontzas, E.; Froudakis, G. E. Multi-scale theoretical investigation of hydrogen storage in covalent organic frameworks. *Nanoscale* **2011**, *3*, 856–869.

(34) Stephens, P. J.; Devlin, F. J.; Chabalowski, C. F.; Frisch, M. J. Ab Initio Calculation of Vibrational Absorption and Circular Dichroism Spectra Using Density Functional Force Fields. *The Journal of Physical Chemistry* **1994**, *98*, 11623–11627.

(35) Weigend, F.; Haser, M.; Patzelt, H.; Ahlrichs, R. RI-MP2: optimized auxiliary basis sets and demonstration of efficiency. *Chemical Physics Letters* **1998**, *294*, 143 – 152.

(36) Grimme, S.; Ehrlich, S.; Goerigk, L. Effect of the damping function in dispersion corrected density functional theory. *Journal of Computational Chemistry* **2011**, *32*, 1456–1465.

(37) Becke, A. D.; Johnson, E. R. Exchange-hole dipole moment and the dispersion interaction. *The Journal of Chemical Physics* **2005**, *122*, 154104.

(38) Boys, S.; Bernardi, F. The calculation of small molecular interactions by the differences of separate total energies. Some procedures with reduced errors. *Molecular Physics* **1970**, *19*, 553–566.

(39) TURBOMOLE V7.1 2016, a development of University of Karlsruhe and Forschungszentrum Karlsruhe GmbH, 1989-2007, TURBOMOLE GmbH, since 2007; available from `http://www.turbomole.com`.

(40) Dovesi, R.; Orlando, R.; Civalleri, B.; Roetti, C.; Saunders, V. R.; Zicovich-Wilson, C. M. CRYSTAL: a computational tool for the ab initio study of the electronic properties of crystals. *Zeitschrift fur Kristallographie - Crystalline Materials* **2009**, *220*, 571–573.

(41) Perdew, J. P.; Burke, K.; Ernzerhof, M. Generalized Gradient Approximation Made Simple. *Phys. Rev. Lett.* **1996**, *77*, 3865–3868.

(42) Peintinger, M. F.; Oliveira, D. V.; Bredow, T. Consistent Gaussian basis sets of triple-zeta valence with polarization quality for solid-state calculations. *Journal of Computational Chemistry* **2013**, *34*, 451–459.

(43) Zagorodniy, K.; Seifert, G.; Hermann, H. Metal-organic frameworks as promising candidates for future ultralow-k dielectrics. *Applied Physics Letters* **2010**, *97*.

(44) Alvaro, M.; Carbonell, E.; Ferrer, B.; i Xamena, F. X. L.; Garcia, H. Semiconductor Behavior of a Metal-Organic Framework (MOF). *Chemistry - A European Journal* **2007**, *13*, 5106–5112.

(45) Baldereschi, A.; Baroni, S.; Resta, R. Band Offsets in Lattice-Matched Heterojunctions: A Model and First-Principles Calculations for GaAs/AlAs. *Phys. Rev. Lett.* **1988**, *61*, 734–737.

(46) Bilc, D.; Orlando, R.; Shaltaf, R.; Rignanese, G.-M.; Íñiguez, J.; Ghosez, P. Hybrid exchange-correlation functional for accurate prediction of the electronic and structural properties of ferroelectric oxides. *Phys. Rev. B* **2008**, *77*, 165107.

(47) Dubbeldam, D.; Calero, S.; Ellis, D. E.; Snurr, R. Q. RASPA: molecular simulation software for adsorption and diffusion in flexible nanoporous materials. *Molecular Simulation* **2016**, *42*, 81–101.

(48) Mayo, S. L.; Olafson, B. D.; Goddard, W. A. DREIDING: a generic force field for molecular simulations. *The Journal of Physical Chemistry* **1990**, *94*, 8897–8909.

(49) Sowlati-Hashjin, S.; Matta, C. F. The chemical bond in external electric fields: Energies, geometries, and vibrational Stark shifts of diatomic molecules. *The Journal of Chemical Physics* **2013**, *139*, 144101.

(50) Souza, I.; Íñiguez, J.; Vanderbilt, D. First-Principles Approach to Insulators in Finite Electric Fields. *Phys. Rev. Lett.* **2002**, *89*, 117602.

(51) Kittel, C. *Introduction to Solid State Physics*, 7th ed.; John Wiley & Sons, Inc.: New York, 1996.

(52) Kuc, A.; Heine, T.; Seifert, G.; Duarte, H. A. On the nature of the interaction between H2 and metal-organic frameworks. *Theoretical Chemistry Accounts* **2008**, *120*, 543–550.

(53) Stone, A. *The Theory of Intermolecular Forces*; International Series of Monographs on Chemistry; Clarendon Press, 1997.

(54) Zhao, D.; Yuan, D.; Zhou, H.-C. The current status of hydrogen storage in metal-organic frameworks. *Energy Environ. Sci.* **2008**, *1*, 222–235.

(55) Fischer, M.; Hoffmann, F.; Fröba, M. Molecular simulation of hydrogen adsorption in metal-organic frameworks. *Colloids and Surfaces A: Physicochemical and Engineering Aspects* **2010**, *357*, 35 – 42, Characterization of Porous Materials: From Angstroms to MillimetersA Collection of Selected Papers presented at the Fifth International Workshop CPM-5.

(56) Darkrim, F.; Levesque, D. Monte Carlo simulations of hydrogen adsorption in single-walled carbon nanotubes. *The Journal of Chemical Physics* **1998**, *109*, 4981–4984.

(57) Zhang, W.; Xiong, R.-G. Ferroelectric Metal-Organic Frameworks. *Chemical Reviews* **2012**, *112*, 1163–1195, PMID: 21939288.

(58) Frenkel, D., Smit, B., Eds. *Understanding Molecular Simulation: From Algorithms to Applications*, 2nd ed.; Academic Press, Inc.: Orlando, FL, USA, 2002.

5 Supporting Information for Electrically Enhanced Hydrogen Adsorption in Metal-Organic Frameworks

We include additional *ab initio* simulations to support the idea that the dipole-dipole interaction is the most important contribution to electrically induced uptake, while higher order contributions cancel out when statistical averaging is performed. We show PES scans for H_2 with perpendicular orientation with respect to the binding sites, and we compute the binding energies of H_2 to these sites. We also present additional benchmarking of the cluster calculations for the binding energies with different functionals. We include the parameters used in the GCMC simulations such as charges, Born charges, dispersion coefficients. We add a pictorial explanation of the polarized model for IRMOF-1 used in the simulations.

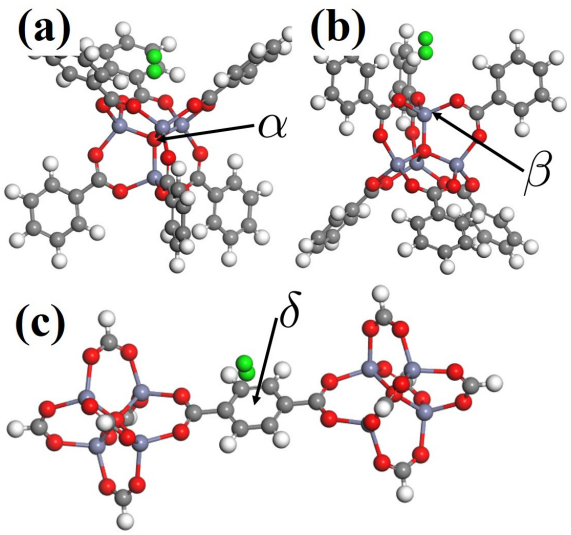

Figure 4: Models used for calculations of the binding energies of H_2 at the sites α, β and δ in IRMOF-1. The direction of the applied field $E_0\hat{z}$ is perpendicular to the binding positions. The Zn, C, O and H atoms of the fragments are colored purple, gray, red and white, respectively. The adsorbed H_2 is colored green.

5.1 Quantum chemistry calculations

We have computed the binding energies of H_2 at the sites α, β and δ in IRMOF-1 under the influence of applied electric field and compared the results with the case of zero field. For the binding energy calculations, we considered, as previously done in the literature,[28] the models presented in Fig. 4. In the figure, the z-axis is the direction joining the center of H_2 molecule to the each binding site.

The electric field is considered along the z-axis. The dimer formed by the IRMOF-1 molecular fragment and H_2 is relaxed until the hydrogen reaches its equilibrium position. To make sure the optimized structures correspond to an energy minimum, the dimers are optimized with the hydrogen initially oriented either along the z-axis or in the horizontal xy-plane. After structural optimization is performed, the calculations are corrected for BSSE errors using the counterpoise method.

Table 1: Binding energies in kJ/mol for the three IRMOF-1 binding sites considered in our calculations. Note that the binding energy for one direction of applied field is larger than the zero field value, while for the opposite direction of the field tends to be smaller (the difference seen for the β site is due to the displacement of H_2 from the initial position. The results in 0-field are consistent with previously reported calculations.[28–30]

Field (a.u.)	E_B^α	E_B^β	E_B^δ
0.0	-7.4	-3.9	-3.8
-0.005	-7.1	-4.8	-4.1
0.005	-8.4	-3.9	-3.5

The models shown in Fig. 4 for the α, β sites are used in the structural optimizations because the 6 benzene arms prevent the molecule from moving to the site α during the geometry optimization steps. The benzene arms can be replaced by hydrogen atoms in the case of potential energy scans done to obtain the dependence of the energy on the distance to the binding site, along the z-axis as in the main text.

The binding energies, obtained for the optimized structures, are presented in the Table 1. The superscript corresponding to each energy in the table references the subsection which lists the XYZ-file containing the optimized structure of each dimer.

As in the main text, the ab initio calculations are performed at the B3-LYP[34] level of theory with the def2-TZVP[35] basis set. Dispersion corrections[36] with Becke-Johnson damping are taken into account. We also correct for the basis set superposition errors using the counterpoise method.[38] The structural optimizations of monomers and dimers have considered 10^{-8}a.u. tolerance for the energy convergence and 10^{-4}a.u. for the geometry convergence. The calculations are performed using the TURBOMOLE software package.[39]

Similar to Fig. 1 in the main text, we have performed *ab initio* simulations in the case the H_2 is perpendicular to the z-direction. In Fig. 5, the positive direction for the applied field is considered the $\hat{z}$-direction. The horizontal axis of the graph represents the distance between the center of the H_2 molecule and a) center of the benzene ring, b) the μ_3-O atom in the center of the SBU, c) the Zn atom above the μ_3-O from the center of the SBU.

As it is shown in Fig. 5, the qualitative behavior of the binding energy in applied electric field persists. In other words, for a field direction the binding is enhanced, while for the other, is lower. To explain this behavior, we can follow the same qualitative argument as in the main text: the dipole-dipole (DD) contribution is small but always attractive, while the dipole-quadrupole (DQ and QD) contributions are larger, but change sign with the electric field. It is important to mention here that the H_2 dipole is smaller if the field is perpendicular to it. Therefore, the dipole-dipole interaction, between H_2 and binding sites, is smaller than for H_2 oriented parallel to the z-axis.

Quadrupoles in electric field. As discussed in the main text, H_2 quadrupole changes only slightly as electric field is applied. This justifies the approximation we used to estimate the additional electrostatic interaction energy between hydrogen and the binding sites on

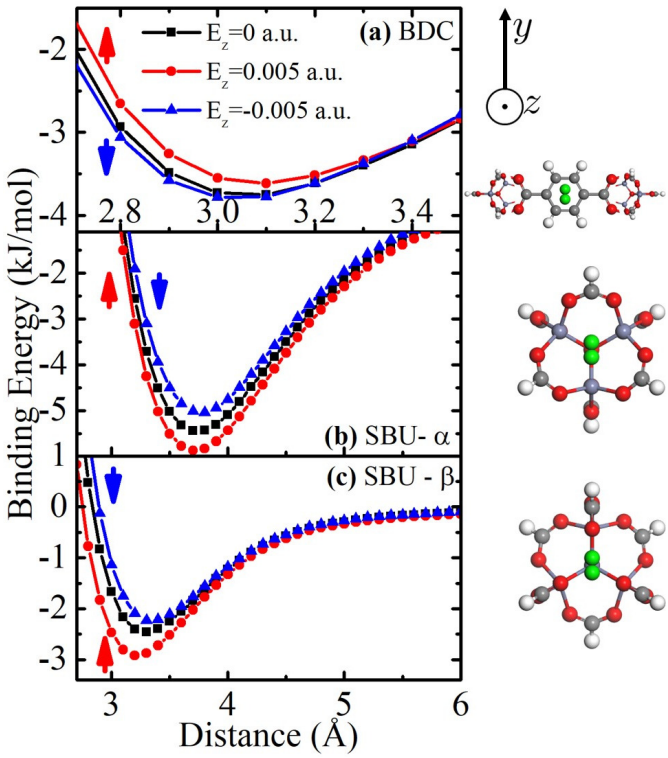

Figure 5: Potential energy curves for H_2 perpendicular to the z-axis adsorbed above a) the δ-site on the BDC linker, b) the α-site, c) the β-site on the SBU. As in the main text, the models used in the calculations for the α and β sites are next to the graphs. But, the model used for the δ site calculation is the one shown in Fig. 4c, which contains the two hydrogen terminated SBUs connected by the linker. The Zn, C, O and H atoms of the fragments are colored purple, gray, red and white, respectively.

IRMOF-1 in the presence of the applied electric field. The H_2 traceless quadrupole in zero field is $\Theta = \mathrm{diag}(-0.20447, -0.20447, 0.40894)$. For field parallel to the H_2 axis, the quadrupole is $\Theta = \mathrm{diag}(-0.20423, -0.20423, 0.40846)$, and if the field E_0 is perpendicular to the H_2 axis $\Theta = \mathrm{diag}(-0.204465, -0.20465, 0.408930)$. The quadrupoles of the MOF fragments are also insensitive to the applied field. The traceless quadrupole of benzene, which is representative for the BDC linker, is, in zero field, $\Theta \approx \mathrm{diag}(2.87112, 2.87226, -5.74338)$, where we neglected the off-diagonal terms that are four orders of magnitude smaller than the diagonal. Applying electric field perpendicular to the center of the benzene, this

quadrupole changes only slightly to $\Theta \approx \mathrm{diag}(2.87976, 2.88074, -5.76050)$.

Additional benchmarking: the choice of functionals. Functionals such as PBE and B3-LYP have been previously used in studying hydrogen adsorption in IRMOF-1.[28,30,52] Recently, a benchmarking study,[29] performed on IRMOF-1, concluded that the meta-GGA functional M06-2x[54] gives more precise results than the other two. Thus, we repeated the calculations of the binding energy of the H_2 to the binding sites considered in Fig. 1 of the manuscript. These calculations were performed using TURBOMOLE at the M06-2x/def2-TZVP level of the theory. The calculations use the counterpoise method to correct for the BSSE errors. Dispersion corrections are also taken account in the simulation. Fig. 6 presents these results side by side with the results of Fig. 1 in the manuscript, which were obtained using the B3-LYP functional. To perform these energy vs distance scans, the monomers (H_2 and MOF fragments) were optimized prior the calculation with the same functional and electric field used in the scans.

Comparing the two panels of Fig. 6, we can see that the results differ both quantitatively and qualitatively. To explain the quantitative differences one should carry out additional benchmarking calculations in electric field using more computationally demanding, but also more precise methods such as MP2. For the calculations performed with the M06-2x functional, shown in the right panel of Fig. 6a, the binding energy for the δ-site increases for positive electric field, and decreases for negative electric field. Qualitatively, this is the opposite of the result obtained using the B3-LYP functional, and expected from the electrostatics arguments invoked in the manuscript. Nonetheless, if the same calculation is performed on a simpler model of the α-site, the results are qualitatively the same as expected from the electrostatics considerations. In this case, presented in Fig. 7, the results obtained from the GGA functionals PBE and B3-LYP agree with the results obtained for the meta-GGA functionals M06-2x and M06.

The GCMC calculations presented in the paper are consider only the induced polarization (effective Born charges) effect of the electric field on the MOF. The effect of the electric field on the exchange-correlation terms of the interaction between the MOF and H_2 is not included, as the Lennard-Jones dispersion potential is parametrized in the absence of the electric field. This parametrization works well in the zero field case. However, if stronger polarization effects are present, this simple model should be revised to include i) more precise calculations of the effective Born charges, ii) a field-dependent parametrization of the exchange-correlation effects. The latter could prove a daunting task due to the asymmetry introduced by the electric field.

5.2 Parameters for the GCMC simulations

Parameters for H_2. In zero field, the H_2 is modeled[56] as a quadrupole with $q \approx 0.468e$ on the hydrogen atoms and $-2q$ charge in the center of the molecule. For H_2 parallel to the applied field, the charges are $q \pm \delta q$ on the H atoms and $-2q$ in the center of the molecule. $\delta q = 0.023e$ is chosen so that the dipole of H_2 along its axis is $p_{\parallel} = 0.033$a.u.. The model for H_2 polarized perpendicular to its axis has the same charges as the unpolarized model, but its center charge is displaced perpendicular to the molecule's axis by $\delta d = 0.0074$Å. This is chosen to reproduce the dipole moment $p_{\perp} = 0.013$a.u. induced by electric field E_0 perpendicular to the molecule's axis.

Parameters of the unpolarized IRMOF-1 model. There are 7 inequivalent atoms in IRMOF-1 unit cell. Each of these has a partial charge q_i. The corresponding Lennard-Jones coefficients C_6^i, C_{12}^i are taken from the DREIDING force field parameters[48] Table 2a contains the partial charges and Lennard-Jones coefficients used in our calculations for IRMOF-1. The position of the other 417 equivalent atoms in the IRMOF-1 unit cell can be obtained by applying symmetry transforms S from the space group 225 of IRMOF-1.

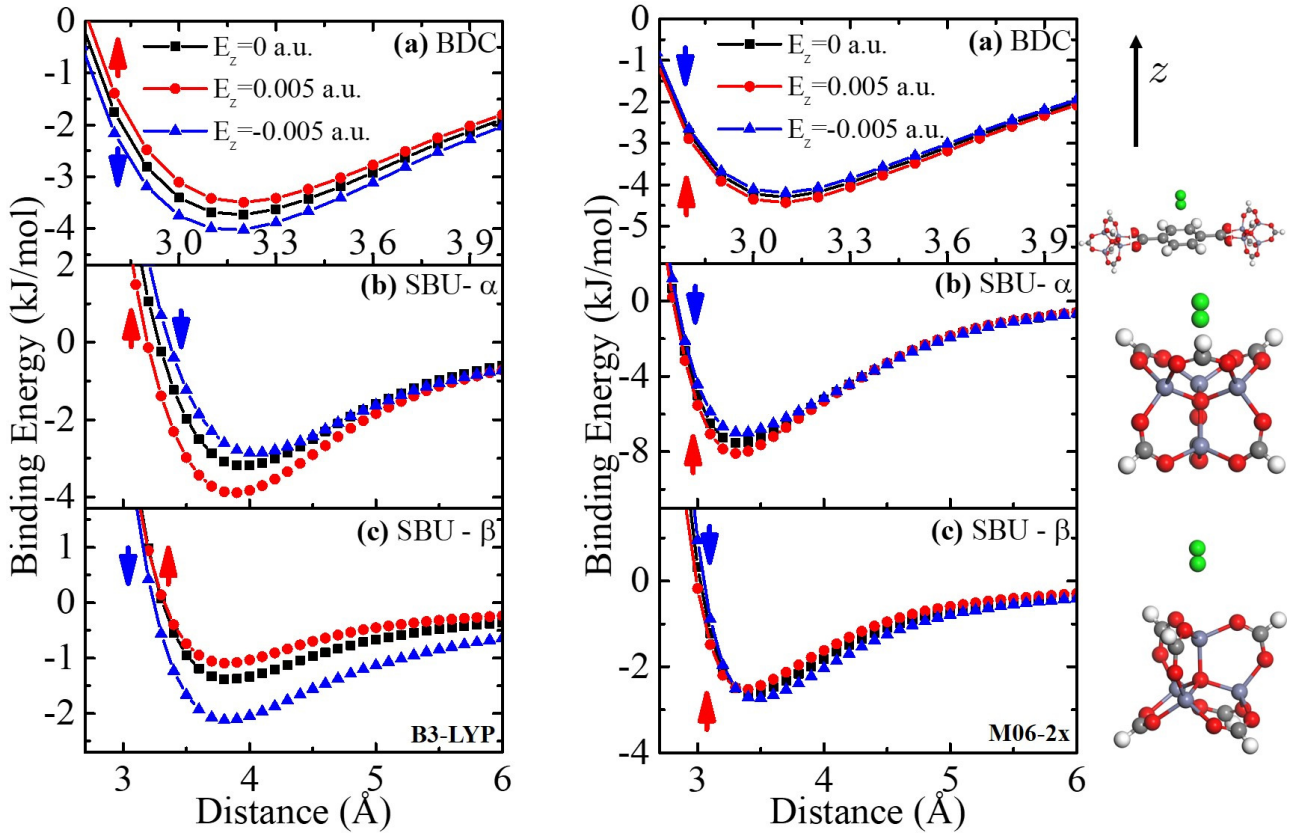

Figure 6: The binding energy as a function of the distance of H_2 to a) the δ-site located above the benzene ring of the BDC linker, b) the α-site and the c) β-site on the SBU. The left panel contains the data presented in Fig. 1 of the main manuscript which was obtained with the B3-LYP functional, while the right panel represents the results of the same calculation performed using the M06-2x functional. The Zn, C, O and H atoms of the fragments are colored purple, gray, red and white, respectively. The adsorbed H_2 is colored green.

Parameters of the polarized IRMOF-1 model. The polarized IRMOF-1 model uses the partial charges and Lennard-Jones coefficients presented in Table. 2a. To include the polarization effects, we computed the Born charges Z_i^* for each of the inequivalent MOF atoms, as explained in the main text. The point dipole corresponding to an atom i is $\mathbf{p}_i = Z_i^*(\mathbf{R}_i(E_0) - \mathbf{R}_i)$, where $\mathbf{R}_i$ is the atomic position of the atom in zero field, while $\mathbf{R}_i(E_0)$ is the atomic position of the atom i in field $E_0\hat{z}$. As the Born charge is a tensor, the induced dipole of the atom i is not necessarily parallel to the field. The calculated Born charges are shown in Table 3 for the 7 inequivalent atoms in the IRMOF-1 fcc unit cell. From these Born charges, one can obtain the Born charges for any equivalent atoms in the unit cell using the symmetry operations S from the space group 225 of IRMOF-1. If Z_i^* of atom i is known, $Z_j^* = SZ_i^*S^\dagger$ for the equivalent atom j. The periodic system DFT calculations, from which we obtained Born charges, atomic positions, and lattice constants, discussed in the next section, were performed using the software CRYSTAL[40] as described in the main text.

IRMOF-1 model for GCMC simulations. The GCMC simulations were performed by considering a 424-atom fcc IRMOF-1 cell. In this cell, each atom has its charge q_i as shown in Table 2a. To create a model for IRMOF-1 that includes the electrically induced polarization, we place a dummy atomic site next to each atom as shown in Fig. 8. In this model, charges $Q_i > 0$ are placed on the dummy site and $q_i - Q_i$ are placed on the atomic site i. $\mathbf{R}_i$ is the position of the site i as obtained by lattice relaxation in zero field. The dummy site is placed at $\mathbf{R}_i + \mathbf{d}_i$,

Table 2: Parameters for GCMC in zero field case. a) Lennard-Jones coefficients and partial charges for the inequivalent atoms in IRMOF-1 unit cell. The reduced coordinate for these atoms are given, where $a = b = c$ for IRMOF-1 cubic cell. b) partial charges and Lennard-Jones coefficients for the adsorbate. Note that the IRMOF-1 atoms only interact with the center of mass H_{COM} of the H_2 via Lennard-Jones dispersion potentials.

(a)	IRMOF-1						
Label	Type	x/a	y/b	z/c	Charge	C_6	C_{12}
Zn1	Zn	0.2936	0.2064	0.2064	1.5332	27.6760	4.0454
O1	O	0.2500	0.2500	0.2500	-1.8572	48.1562	3.0337
O2	O	0.2809	0.2191	0.1331	-0.7817	48.1562	3.0337
C1	C	0.2500	0.2500	0.1105	0.7364	47.0000	3.4726
C2	C	0.2500	0.2500	0.0534	0.0882	47.8600	3.4700
C3	C	0.2828	0.2172	0.0265	-0.1504	47.8600	3.4700
H1	H	0.3082	0.1918	0.0481	0.1634	7.6500	2.8500
(b)	H_2						
H_{atom}	H	-	-	-	0.4680	-	-
H_{COM}	H	-	-	-	0.9360	36.7000	2.9580

Table 3: The Born charges obtained for the IRMOF-1 atoms as discussed in the main text.

Label	Type	Z^*_{xx}	Z^*_{xy}	Z^*_{xz}	Z^*_{yx}	Z^*_{yy}	Z^*_{yz}	Z^*_{zx}	Z^*_{zy}	Z^*_{zz}
Zn1	Zn	2.15	0.22	0.22	0.22	2.15	-0.22	-0.22	-0.22	2.15
O1	O	-1.85	0.0	0.0	0.0	-1.85	0.0	0.0	0.0	-1.85
O2	O	-0.99	0.44	-0.47	0.44	-0.99	0.47	-0.64	0.64	-2.07
C1	C	1.18	-0.91	0.0	-0.91	1.18	0.0	0.0	0.0	3.18
C2	C	-0.03	0.06	0.0	0.06	-0.03	0.0	0.0	0.0	-1.1
C3	C	-0.03	-0.06	0.17	-0.06	-0.03	-0.16	-0.06	0.06	-0.03
H1	H	0.06	0.06	-0.03	0.06	0.06	0.03	-0.06	0.06	0.11

where the vector $\mathbf{d}_i$ is chosen so that $\mathbf{p}_i = Q_i\mathbf{d}_i$. The distance between the dummy position and its corresponding atom i has been chosen constant $d_i = 0.27$Å. One can see from the figure that the dummy atoms are not only displaced along the z-axis with respect to the positions of their corresponding atoms. This is consistent with the fact that the polarization induced by the applied field is not necessarily parallel to the applied field since the Born charge is a tensor with off-diagonal components. The GCMC simulations are performed with the RASPA2 software.[47] For the zero field case, we use the 424-atom fcc unit cell of the MOF, while for the field along z-axis, we use the unit cell with the extra 424 dummy sites as shown in Fig. 8.

Cancellation of the quadrupole-dipole effects on adsorption. We argued in the main text that the dipole-quadrupole contributions to the interaction energy between H_2 and its binding sites in IRMOF-1 do not affect the uptake. In IRMOF-1, and any MOF with reflection symmetry, we can obtain an identical site to a given site by simply performing a reflection. Assume the electric field is turned on and is perpendicular to the reflection plane. The hydrogen can bind to both sites, the first site, and the one obtained by reflection. On one of the sites, the dipole-quadrupole interaction will have one sign, while on the other, it will have the opposite sign. Note that the dipole-dipole contribution would always have the same sign on both sites.

The algorithm for the GCMC simulations[58]

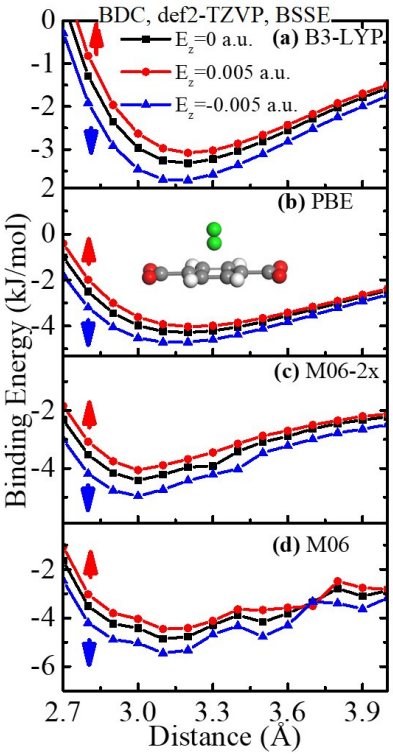

Figure 7: Comparison of the binding energy of H_2 to the δ-site on the BDC linker, calculated with a) PBE, b) B3-LYP, c) M06-2x, and d) M06 functionals. The results are BSSE corrected. All the calculations use a H_2 molecule and a BDC fragment initially optimized with B3-LYP in zero electric field. The C, O and H atoms of the MOF fragment modeling the δ-site are colored gray, red and white, respectively. The adsorbed H_2 is colored green.

implies the generation of a starting configuration for the H_2 present in the MOF cell. Once that is generated, a number N of cycles are performed, until, on average, the energy and the number of particles inside the selected MOF cell does not change anymore. During a cycle, moves such as insertion, deletions, translations and rotations of H_2 molecules are performed. The averaging is done every n cycles, over the last n cycles, including the current one. Average energies and number of adsorbate particles are computed. If these averages do not differ significantly from the previous averages, the GCMC calculation is converged.

Assume we perform n cycles and compute average densities and energies at the end. Let us consider a site, for instance, the site α of

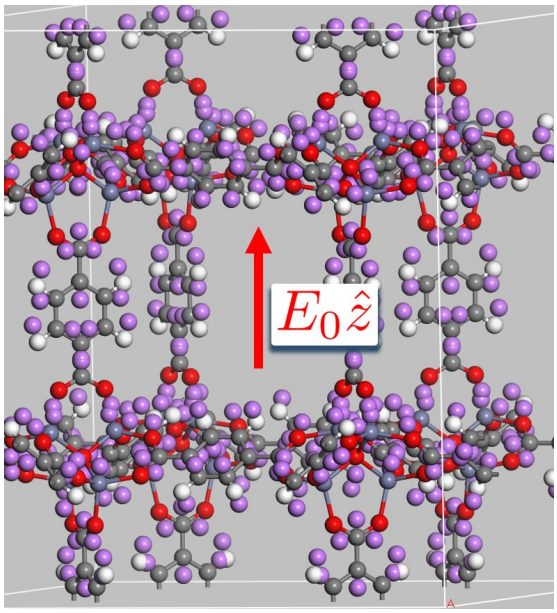

Figure 8: Pictorial representation of the polarized model for IRMOF-1. The Zn, C, O and H and dummy atoms are colored purple, grey, red, white, and magenta, respectively.

IRMOF-1 as in Fig. 4. Another identical site α' can be obtained by performing a reflection operation allowed by the crystal symmetry. We will have configurations in which i) none of the two sites is occupied, ii) only one of the sites is occupied, iii) both sites are occupied. The situation i) is equally probable for both directions of the applied electric field $\mathbf{E}$.

In the situation ii) for one field direction, we have either site α, or site α' occupied. Let us label the binding energy at these sites $E_B^{\alpha}(\mathbf{E})$, or $E_B^{\alpha'}(\mathbf{E})$. Neglecting the relatively small dipole-dipole interaction, we have $E_B^{\alpha}(\mathbf{E}) \approx E_B^{\alpha'}(-\mathbf{E})$, as the main contribution to the energy coming from the dipole-quadrupole interaction changes sign with electric field. That means the configuration with electric field $\mathbf{E}$ and site α occupied is as probable as the one with electric field $-\mathbf{E}$ and site α' occupied, if we neglect the dipole-dipole interactions. As a result, there will be an equal number of configurations with one of the sites occupied for both directions of the applied field.

In the situation iii), in which both sites are occupied, we can argue that the probability to arrive at such configuration, from a configuration in which they are unoccupied is, for a given

direction of the field, $P(E) = P_\alpha(\mathbf{E})P_{\alpha'}(\mathbf{E})$, where the probability to occupy the site by performing a move is[58] $P_\alpha(\mathbf{E}) = e^{-\beta E_B^\alpha(\mathbf{E})}$. Then, the probability of obtaining a configuration with both sites occupied is equal for both field directions, and very close to the one obtained for zero field, if the dipole-dipole interaction is weak.